

Profilin-Dependent Nucleation and Assembly of Actin Filaments Controls Cell Elongation in Arabidopsis¹[OPEN]

Lingyan Cao, Jessica L. Henty-Ridilla², Laurent Blanchoin, and Christopher J. Staiger*

Department of Biological Sciences, Purdue University, West Lafayette, Indiana 47907–2064 (L.C., J.L.H.-R., C.J.S.); and Institut de Recherches en Technologie et Sciences pour le Vivant, Commissariat à l'Énergie Atomique/Centre National de la Recherche Scientifique/Institut National de la Recherche Agronomique/Université Joseph Fourier, CEA Grenoble, F–38054 Grenoble cedex 9, France (L.B.)

ORCID ID: 0000-0002-7203-8791 (J.L.H.-R.).

Actin filaments in plant cells are incredibly dynamic; they undergo incessant remodeling and assembly or disassembly within seconds. These dynamic events are choreographed by a plethora of actin-binding proteins, but the exact mechanisms are poorly understood. Here, we dissect the contribution of Arabidopsis (*Arabidopsis thaliana*) PROFILIN1 (PRF1), a conserved actin monomer-binding protein, to actin organization and single filament dynamics during axial cell expansion of living epidermal cells. We found that reduced PRF1 levels enhanced cell and organ growth. Surprisingly, we observed that the overall frequency of nucleation events in *prf1* mutants was dramatically decreased and that a subpopulation of actin filaments that assemble at high rates was reduced. To test whether profilin cooperates with plant formin proteins to execute actin nucleation and rapid filament elongation in cells, we used a pharmacological approach. Here, we used Small Molecule Inhibitor of Formin FH2 (SMIFH2), after validating its mode of action on a plant formin *in vitro*, and observed a reduced nucleation frequency of actin filaments in live cells. Treatment of wild-type epidermal cells with SMIFH2 mimicked the phenotype of *prf1* mutants, and the nucleation frequency in *prf1-2* mutant was completely insensitive to these treatments. Our data provide compelling evidence that PRF1 coordinates the stochastic dynamic properties of actin filaments by modulating formin-mediated actin nucleation and assembly during plant cell expansion.

The actin cytoskeleton provides tracks for the deposition of cell wall materials and plays important roles during many cellular processes, such as cell expansion and morphogenesis, vesicle trafficking, and the response to biotic and abiotic signals (Baskin, 2005; Smith and Oppenheimer, 2005; Szymanski and Cosgrove, 2009; Ehrhardt and Bezanilla, 2013; Rounds and Bezanilla, 2013). Plant cells respond to diverse internal and external stimuli by regulating the turnover and rearrangement of actin cytoskeleton networks in the cytoplasm (Staiger, 2000; Pleskot et al., 2013). How these actin rearrangements sense the cellular environment and what accessory proteins modulate specific aspects of remodeling remain an area of active investigation (Henty-Ridilla et al., 2013; Li et al., 2014a, 2015).

Using high spatial and temporal resolution imaging afforded by variable-angle epifluorescence microscopy (VAEM; Konopka and Bednarek, 2008), we quantified the behavior of actin filaments in Arabidopsis (*Arabidopsis thaliana*) hypocotyl epidermal cells (Staiger et al., 2009). There are two types of actin filament arrays in the cortical cytoplasm of epidermal cells: bundles and single filaments. Generally, actin bundles are stable with higher pixel intensity values, whereas individual actin filaments are fainter, more ephemeral, and constantly undergo rapid assembly and disassembly through a mechanism that has been defined as “stochastic dynamics” (Staiger et al., 2009; Henty et al., 2011; Li et al., 2012, 2015). Elongating actin filaments in the cortical cytoskeleton originate from three distinct locations: the ends of preexisting actin filaments, the side of filaments or bundles, and *de novo* in the cytoplasm. Plant actin filaments elongate at rates of 1.6 to 3.4 $\mu\text{m/s}$, which is the fastest assembly reported in eukaryotic cells. Distinct from the mechanism of treadmilling and fast depolymerization *in vitro*, however, the disassembly of single actin filaments occurs predominately through prolific severing activity (Staiger et al., 2009; Smertenko et al., 2010; Henty et al., 2011). A commonly held view is that the dynamic actin network in plant cells is regulated by the activities of conserved and novel actin-binding proteins (ABPs). Through reverse-genetic approaches and state-of-the-art imaging modalities, we and others have demonstrated that several key

¹ This work was supported by the U.S. National Science Foundation (grant no. IOS-1021185 to C.J.S.).

² Present address: Department of Biology, Brandeis University, Waltham, MA 02454.

* Address correspondence to staiger@purdue.edu.

The author responsible for distribution of materials integral to the findings presented in this article in accordance with the policy described in the Instructions for Authors (www.plantphysiol.org) is: Christopher J. Staiger (staiger@purdue.edu).

L.C., J.L.H.-R., L.B., and C.J.S. conceptualized and designed the research; L.C. and J.L.H.-R. performed the research and analyzed data; L.C. and C.J.S. wrote the article.

[OPEN] Articles can be viewed without a subscription.

www.plantphysiol.org/cgi/doi/10.1104/pp.15.01321

ABPs are involved in the regulation of stochastic actin dynamic properties in a wide variety of plants and cell types (Thomas, 2012; Henty-Ridilla et al., 2013; Li et al., 2014a, 2015). Through these efforts, the field has developed a working model for the molecular mechanisms that underpin actin organization and dynamics in plant cells (Li et al., 2015).

Profilin is a small (12–15 kD), conserved actin-monomer binding protein present in all eukaryotic cells (dos Remedios et al., 2003). Profilin binds to actin by forming a 1:1 complex with globular (G-)actin, suppresses spontaneous actin nucleation, and inhibits monomer addition at filament pointed ends (Blanchoin et al., 2014). The consequences of profilin activity on actin filament turnover differ based on cellular conditions and the presence of other ABPs. In vitro studies show that the profilin-actin complex associates with the barbed ends of filaments and promotes actin polymerization by lowering the critical concentration and increasing nucleotide exchange on G-actin (Pollard and Cooper, 1984; Pantaloni and Carlier, 1993). When barbed ends are occupied by capping protein, profilin acts as an actin-monomer sequestering protein. These opposing effects of profilin might be a regulatory mechanism for profilin modulation of actin dynamics in cells. In addition to actin, profilin interacts with Pro-rich proteins, as well as polyphosphoinositide lipids in vitro (Machesky et al., 1994). Formin is an ABP that mediates both actin nucleation and processive elongation using the pool of profilin-actin complexes (Blanchoin et al., 2010). The primary sequence of formin includes a Pro-rich domain, named Formin Homology1 (FH1). Evidence from fission and budding yeast shows that profilin can increase filament elongation rates by binding to the FH1 domain (Kovar et al., 2003; Moseley and Goode, 2005; Kovar, 2006). The FH1 domain of Arabidopsis FORMIN1 (AtFH1) is also reported to modulate actin nucleation and polymerization in vitro (Michelot et al., 2005). Recently, two groups reported that profilin functions as a gatekeeper during the construction of different actin networks generated by formin or ARP2/3 complex in yeast and mammalian cells (Rotty et al., 2015; Suarez et al., 2015). These studies highlight the importance of profilin regulation in coordinating the different actin arrays present in the same cytoplasm of eukaryotic cells. However, direct evidence for how profilin facilitates formin-mediated actin nucleation or barbed end elongation in cells remains to be established.

Genomic sequencing and isolation of *PROFILIN* (*PRF*) cDNAs from plants reveal that profilin is encoded by a multigene family. For example, moss (*Physcomitrella patens*) has three isoforms (Vidali et al., 2007) and maize (*Zea mays*) has five (Staiger et al., 1993; Kovar et al., 2001). In Arabidopsis, at least five *PRF* genes have been identified (Christensen et al., 1996; Huang et al., 1996; Kandasamy et al., 2002). Studies in maize show that the biochemical properties of profilin isoforms differ in vitro (Kovar et al., 2000). Moreover, the localization of profilin isoforms reveals

organ-specific expression patterns. Detection of protein levels in vivo with isoform-specific profilin antibodies demonstrate that Arabidopsis PRF1, PRF2, and PRF3 are constitutively expressed in vegetative tissues, whereas PRF4 and PRF5 are expressed mainly in flower and pollen tissues (Christensen et al., 1996; Huang et al., 1996; Ma et al., 2005).

Several genetic studies on the functions of profilin in plants have been conducted. Reduction of profilin levels in *P. patens* results in the inhibition of tip growth, disorganization of F-actin, and formation of actin patches (Vidali et al., 2007). Moreover, it was shown that the interaction between profilin and actin or Pro-rich ligands is critical for tip growth in moss. Arabidopsis PRF1 has been demonstrated to be involved in cell elongation, cell shape maintenance, and control of flowering time through overexpression and antisense *PRF1* transgenic plants, and further, the reduction of *PRF1* inhibits the growth of hypocotyls (Ramachandran et al., 2000). However, investigation of a *prf1-1* mutant, which contains a T-DNA insertion in the promoter region of the *PRF1* gene, indicates that cell expansion of seedlings is promoted and that protein levels of PRF1 are regulated by light (McKinney et al., 2001). Recently, Müssar et al. (2015) reported a new Arabidopsis T-DNA insertion allele, *prf1-4*, that shows an obvious dwarf seedling phenotype. To date, however, there has not been a critical examination of the impact of the loss of profilin on the organization and dynamics of bona-fide single actin filaments in vivo.

Here, we use a combination of genetics and live-cell imaging to investigate the role of PRF1 in the control of actin dynamics and its effect on axial cell expansion. We observed a significant decrease in the overall filament nucleation frequency in *prf1* mutants, which is opposite to expectations if profilin suppresses spontaneous nucleation. Through a pharmacological approach, we found that nucleation frequency in wild-type cells treated with a formin inhibitor, SMIFH2, phenocopied *prf1* mutants. We also analyzed the dynamic turnover of individual filaments in *prf1* mutants and observed a significant decrease in the rate of actin filament elongation and maximum length of actin filaments. Specifically, we found that PRF1 favors the growth of a subpopulation of actin filaments that elongate at rates greater than 2 $\mu\text{m/s}$ and similar results were obtained in cells after SMIFH2 treatment. Our results provide compelling evidence that Arabidopsis PRF1 contributes to stochastic actin dynamics by modulating formin-mediated actin nucleation and filament elongation during axial cell expansion.

RESULTS

Arabidopsis *prf1* Mutants Show Enhanced Cell and Organ Growth

In Arabidopsis, there are multiple *PRF* genes expressed in different organs (Christensen et al., 1996;

Huang et al., 1996), among which *PRF1* (At2g19760) has the highest predicted transcript level in dark-grown hypocotyls (Ma et al., 2005). To dissect the function of *PRF1*, two T-DNA insertion mutants (SALK_057718 and SALK_143800) were characterized. Because McKinney et al. (2001) named their *prf1* mutant allele *prf1-1*, here we define two additional mutants as *prf1-2* (SALK_057718) and *prf1-3* (SALK_143800). The *prf1-2* and *prf1-3* alleles contain T-DNA insertions in the first exon and the first intron, respectively, of the *PRF1* genomic DNA sequence (Fig. 1A). To detect the expression level of *PRF1* in wild-type plants and *prf1* mutants, quantitative real-time PCR (qRT-PCR) experiments were performed. The qRT-PCR results showed that *PRF1* transcripts were significantly reduced in both *prf1-2* and *prf1-3* mutants, although minor amounts of PCR products could still be detected (Fig. 1B). To examine the *PRF1* protein levels in *prf1-2* and *prf1-3* mutants, we conducted quantitative immunoblotting of total protein extracts from dark-grown seedlings with anti-AtPRF1 specific monoclonal antibody (Kandasamy et al., 2002). Compared to wild-type siblings, only 4% *PRF1* was detected in *prf1-2* and 40% *PRF1* in *prf1-3* (Fig. 1, C and D). The results indicate that *prf1-2* is a knockout mutant and *prf1-3* is a severe knockdown mutant. To determine whether total actin levels change to compensate for the loss of profilin, we also quantified actin in the same extracts. Total actin protein was not significantly altered in either *prf1* mutant (Fig. 1, C and D).

To detect whether the growth of organs and cells was affected in the *prf1* mutant lines, dark-grown seedlings were examined. At 5-d post germination, dark-grown hypocotyls of *prf1* mutants appeared longer than wild-type controls (Fig. 2A). To quantify these observations, a time course of seedling growth was analyzed. Hypocotyls from both *prf1* mutants were modestly, but significantly, longer than wild-type siblings at the same time points (Figs. 2B and 2C). Hypocotyl growth relies almost exclusively on axial cell expansion, rather than cell division (Gendreau et al., 1997). Therefore, epidermal cell lengths from the apex and base of etiolated hypocotyls were measured in 5-d-old seedlings. Both apical and basal epidermal cells in the *prf1* mutants were significantly longer than were those in wild-type cells (Fig. 2D). Similar results were observed for root growth in the light as well as length of epidermal cells in the elongation zone of *prf1* mutants (Fig. 3, A–D). Altogether, these results indicate that *PRF1* negatively regulates axial cell expansion in etiolated hypocotyls and light-grown roots of Arabidopsis.

Epidermal Cells of *prf1* Mutants Have Less Dense Actin Filament Arrays

To study cytoskeletal organization and dynamics, the actin cytoskeleton reporter comprised of GFP fused with the second actin-binding domain of Arabidopsis FIMBRIN1 (GFP-fABD2; Sheahan et al., 2004) was

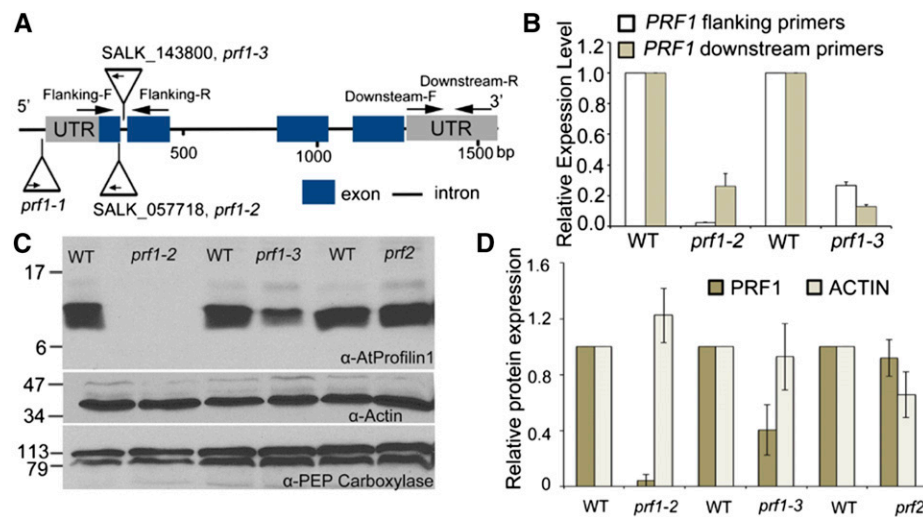


Figure 1. Quantification of *PRF1* expression in *prf1* mutants of Arabidopsis. A, Diagram of *PRF1* gene and T-DNA mutant alleles. Triangles, T-DNA insertions; black lines, introns; blue bars, exons; gray bars, nontranslated regions. Primers used for qRT-PCR in B are labeled with arrows and sequences are given in Supplemental Table S1. B, Relative expression levels of *PRF1* were examined by qRT-PCR analysis of 5-d-old dark-grown seedlings from homozygous *prf1* mutants (*prf1-2*, *prf1-3*) and wild-type (WT) siblings, all marked with GFP-ABD2 reporter. All data were normalized to *GAPD* transcript levels. Values represent mean \pm SE from three biological repeats. C, Representative immunoblot of *PRF1* and actin protein levels in 5-d-old dark-grown seedlings of *prf1* mutants (*prf1-2*, *prf1-3*) and wild-type siblings, all marked with GFP-ABD2. Proteins were detected with anti-AtPRF1 or JLA-20 monoclonal antibodies, respectively. As a loading control, membranes were reprobbed with PEP-carboxylase antibody. D, Quantitative analysis of *PRF1* and actin protein levels measured by densitometry of the profilin or actin band from each genotype and then calculating the fold change compared to wild-type siblings. All data represent mean \pm SE from five biological repeats.

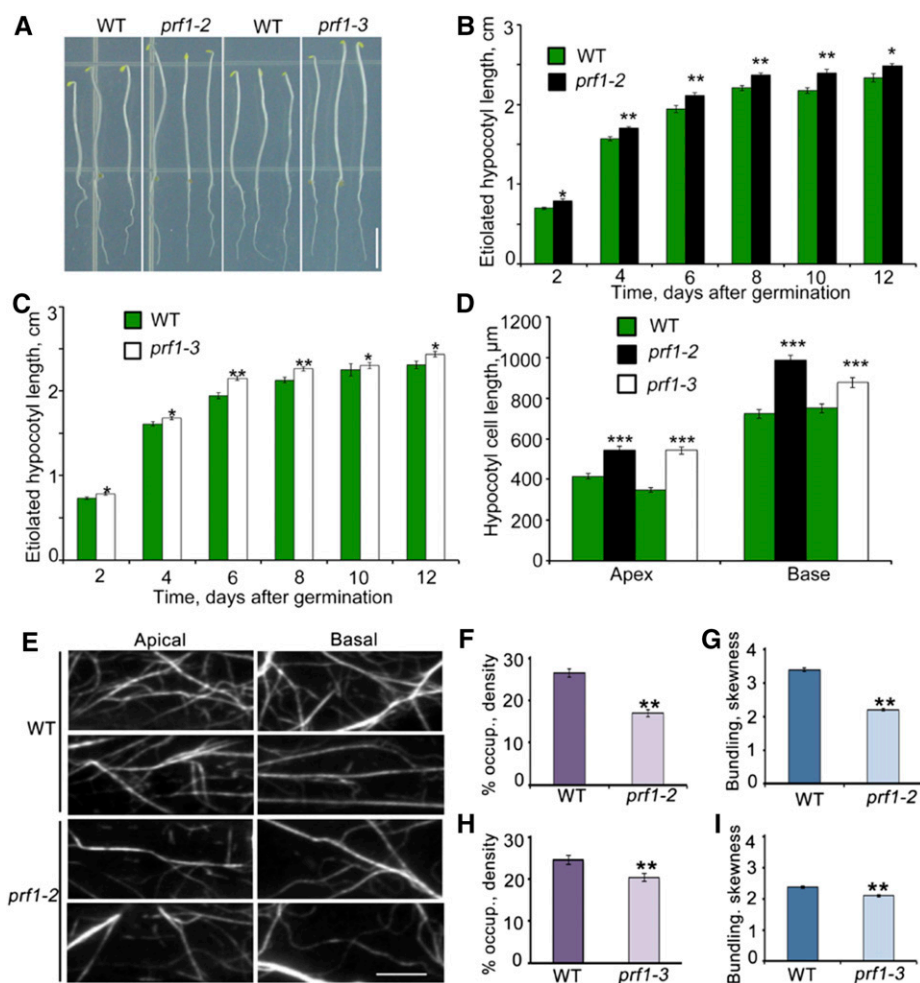


Figure 2. Perturbed actin architecture in *prf1* mutants enhances hypocotyl growth and epidermal cell length in Arabidopsis. A, Representative images of 5-d-old dark-grown seedlings of wild type and *prf1* mutants. Bar, 1 cm. B and C, Etiolated hypocotyls from homozygous *prf1-2* (B) and *prf1-3* (C) mutants were significantly longer than wild-type siblings over a developmental time course. Values represent mean \pm SE, $n \geq 50$ seedlings per genotype, * $P < 0.05$, ** $P < 0.005$, Student's *t* test. D, Epidermal cell lengths were measured from apical and basal regions of 5-d-old etiolated hypocotyls. The average length of epidermal cells from *prf1-2* and *prf1-3* mutants was significantly longer than that of wild-type siblings. Values represent mean \pm SE, $n \geq 50$ cells from at least 10 hypocotyls per genotype, *** $P < 0.001$, Student's *t* test. E, Representative micrographs of epidermal cells from the apical and basal regions of 5-d-old etiolated hypocotyls. Actin filament arrays in *prf1-2* mutant cells appeared to be more sparse and less bundled compared to wild-type cells. Bar, 10 μ m. F and H, Quantitative analysis of the percentage of occupancy (density) of actin filament arrays in epidermal cells from the basal region of hypocotyls. The density of actin arrays in *prf1-2* (F) and *prf1-3* (H) mutants was significantly decreased compared to wild-type siblings. Values represent mean \pm SE, $n \geq 300$ cells from 10 hypocotyls per genotype, ** $P < 0.005$, Student's *t* test. G and I, Quantitative analysis of the extent of filament bundling (skewness) in epidermal cells from the basal region of hypocotyls. The same images used for F and H were analyzed for skewness. Compared to wild type, actin filament arrays in *prf1-2* (G) and *prf1-3* (I) mutants were significantly less bundled.

introduced by crossing a standard line (Staiger et al., 2009) with homozygous *prf1* mutant plants and recovering mutants and wild-type siblings from the F2 generation. To test whether actin cytoskeleton organization was perturbed in *prf1* mutants, images of epidermal cells at the base of 5-d-old dark-grown hypocotyls were collected by VAEM (Konopka and Bednarek, 2008; Staiger et al., 2009). Actin arrays in the *prf1-2* mutant appeared sparse and less bundled compared to wild type (Fig. 2E). To quantitatively analyze these

observations, two metrics, density and skewness, which are defined as the percentage of occupancy of actin filaments and the extent of bundling, respectively, were measured as described previously (Higaki et al., 2010; Henty et al., 2011; Li et al., 2012; Henty-Ridilla et al., 2013). The density of actin filament arrays in homozygous *prf1* mutants was significantly lower than that in wild-type siblings (Fig. 2, F and H), and the extent of bundling was also reduced (Fig. 2, G and I); however, the mutant phenotypes were less severe in

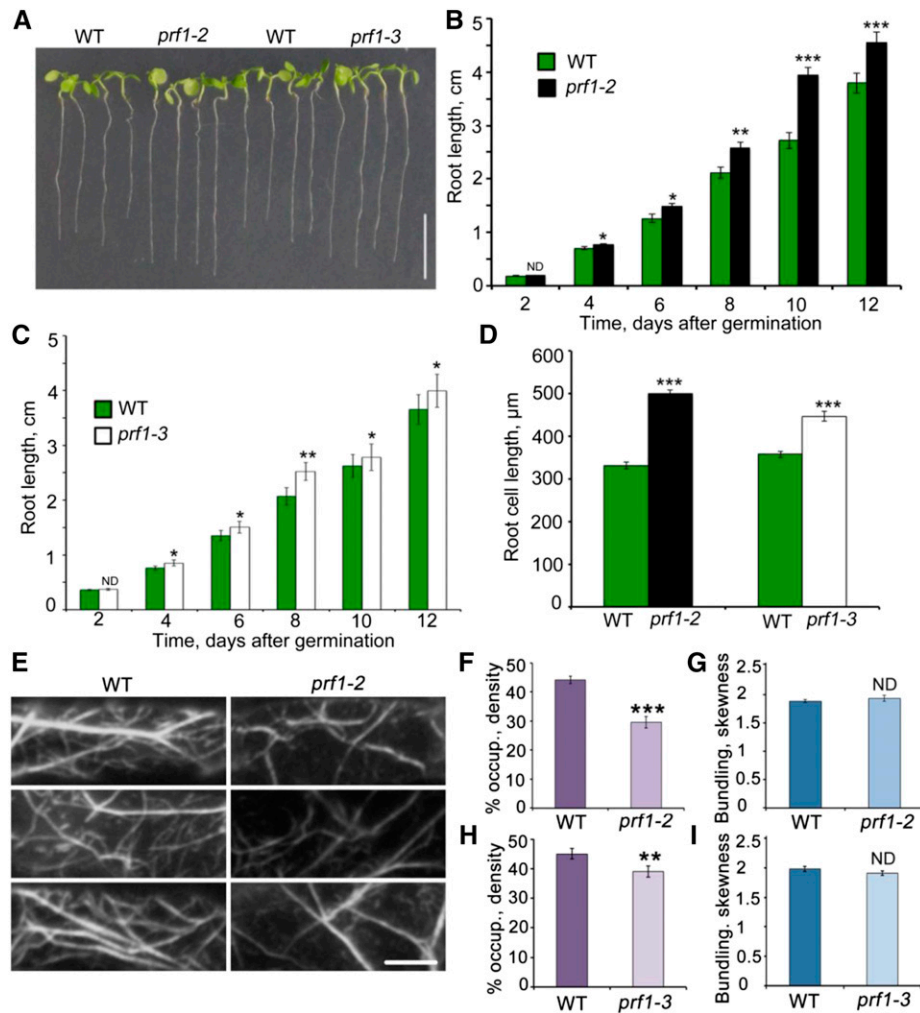


Figure 3. PRF1 is required for normal cortical actin organization in epidermal cells of the root elongation zone. A, Representative images of 7-d-old light-grown roots of wild type and *prf1* mutants. Bar, 1 cm. B and C, Root lengths were measured from light-grown seedlings over a developmental time course. Root lengths of *prf1-2* and *prf1-3* were significantly longer compared to wild-type siblings. Values represent mean \pm SE, $n \geq 50$ roots per genotype, *** $P < 0.001$, ** $P < 0.01$, * $P < 0.05$, ND $P > 0.05$, Student's *t* test. D, Epidermal cell lengths were measured from the elongation zone of 7-d-old light-grown roots. The cell length of *prf1-1* and *prf1-2* mutants was significantly longer compared to wild-type siblings. Values represent mean \pm SE, $n \geq 200$ cells from at least 15 roots, *** $P < 0.001$, Student's *t* test. E, Representative micrographs of epidermal cells from the elongation zone of 7-d-old light-grown roots. Actin filament arrays in *prf1-2* mutant cells appeared to be less dense compared to wild-type cells. Bar, 10 μ m. F and H, Quantitative analysis of the percentage of occupancy (density) of actin filament arrays in epidermal cells from the elongation zone of roots. The density of actin arrays in *prf1-2* (F) and *prf1-3* (H) mutants was significantly decreased compared to wild type. Values represent mean \pm SE, $n \geq 236$ cells from 15 roots per genotype, ** $P < 0.005$, *** $P < 0.001$, Student's *t* test. G and I, Quantitative analysis of the extent of filament bundling (skewness) in epidermal cells from the elongation zone of roots. The same images used for F and H were analyzed for skewness. The extent of bundling of actin filament arrays in *prf1-2* (G) and *prf1-3* (I) mutants was not significantly different compared to wild type ND $P \geq 0.05$.

prf1-3 compared to *prf1-2*. The reduction in apparent density of actin arrays was not due to differences in the reporter between the wild-type and mutant lines or due to lower fluorescence of individual filaments in the *prf1* mutants. Mean fluorescence intensity values for more than 100 single filaments from each genotype showed no significant differences (e.g. 77 ± 25 in wild type versus 84 ± 22 in *prf1-2*; Supplemental Fig. S1). To evaluate whether the reduction in percentage of

occupancy in the *prf1* mutants might be due to a unique interaction between actin filaments and the GFP-fABD2 reporter, we performed rhodamine-phalloidin labeling of formaldehyde fixed cells and imaged them with spinning disk confocal microscopy. Although fixation and phalloidin staining did not give ideal preservation of single actin filaments in hypocotyl epidermal cells, the density of filament arrays was reduced in *prf1-2* and *prf1-3* mutants compared to wild-type cells

(Supplemental Fig. S2). Interestingly, the extent of filament bundling was slightly increased in phalloidin-labeled epidermal cells of *prf1* mutants compared to wild-type, and this again may be due to poor preservation of individual filaments during fixation (Supplemental Fig. S2).

Similar changes in actin array architecture were observed in epidermal cells from the elongation zone of light-grown roots, albeit the extent of filament bundling did not change in *prf1* mutant cells (Fig. 3, E–I). Moreover, epidermal cells from 7-d-old cotyledons of the *prf1* mutants also exhibited a significant reduction in filament density when compared to wild-type siblings (Supplemental Fig. S3). These quantitative analyses demonstrate that PRF1 regulates actin cytoskeleton architecture during axial cell expansion. Specifically, the results show that PRF1 is necessary to generate a dense array of fine actin filaments.

PRF1 Is Involved in Actin Filament Nucleation

The above results imply that PRF1 contributes to axial cell expansion by regulating actin cytoskeleton organization. Previous biochemical studies show that plant profilin is an actin monomer-binding protein that can suppress spontaneous actin nucleation in vitro (Michelot et al., 2005). To further dissect the mechanisms by which PRF1 regulates actin organization in cells, we quantitatively assessed the formation and turnover of single actin filaments (Staiger et al., 2009) in *prf1* mutant cells. Time-lapse movies of epidermal cells from the base of 5-d-old dark-grown hypocotyls were collected by VAEM (Staiger et al., 2009). Previously, we established that growing actin filaments originate from three different locations: the ends of preexisting filaments; the side of another filament or bundle; and de novo in the cytoplasm (Staiger et al., 2009), as shown in Figure 4A. Although we recognize that true filament nucleation involving formation of actin trimers is below the limits of detection by light microscopy, and that elongation from a preexisting filament is not really nucleation per se, for semantic purposes we refer to all of these as nucleation events in the remainder of the text.

To analyze the overall frequency of filament nucleation from the monomer pool, a new metric was developed. All newly initiated, elongating filaments in a $400\ \mu\text{m}^2$ region of interest (ROI) were identified during a 100-s time-lapse series from multiple cells. To minimize the effects of filament abundance or the density of the filament array, we normalized the nucleation frequency to average filament number within the ROI. Compared to wild-type cells (0.56 ± 0.04 events/filament/min), the overall actin nucleation frequency in *prf1-2* mutant cells (0.35 ± 0.03 events/filament/min) was significantly decreased (Fig. 4B). Overall nucleation frequency was also reduced in *prf1-3* (Fig. 4B), confirming that PRF1 promotes, rather than inhibits, actin filament nucleation in cells.

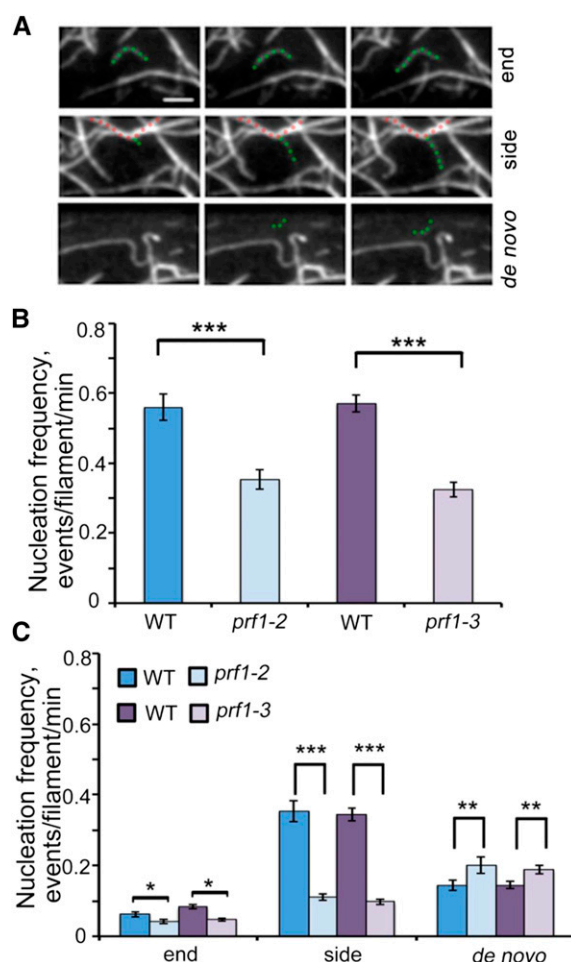


Figure 4. The frequency of filament nucleation events is reduced in *prf1* mutants. A, Three classes of actin filament origin were observed in epidermal cells of 5-d-old dark-grown hypocotyls. Actin filaments initiated from the end of an existing actin filament (top row), the side of an actin filament or bundle (middle row), and de novo in the cytoplasm (Staiger et al., 2009), as shown in Figure 4A. Although we recognize that true filament nucleation involving formation of actin trimers is below the limits of detection by light microscopy, and that elongation from a preexisting filament is not really nucleation per se, for semantic purposes we refer to all of these as nucleation events in the remainder of the text. B, The overall frequency of actin nucleation was defined as the total number of filament origins per filament per minute in a $400\ \mu\text{m}^2$ region of interest. Compared to wild type, total nucleation frequency in *prf1-2* and *prf1-3* was significantly decreased. Values represent mean \pm SE, $n \geq 380$ events per genotype, $***P < 0.001$, Student's *t* test. C, The frequency of actin nucleation types was analyzed using the method indicated in B. Compared to wild type, nucleation frequency from filament sides and ends in *prf1-2* and *prf1-3* were significantly decreased, whereas de novo nucleation frequency was significantly increased compared to wild type. Values represent mean \pm SE, $n \geq 380$ events per genotype or treatment, $***P < 0.001$, $**P < 0.005$, $*P < 0.05$, Student's *t* test.

These data appear to contradict the hypothesis that PRF suppresses spontaneous nucleation in plant cells. To better understand how PRF1 regulates nucleation, we classified nucleation frequency into three categories based on filament origins. Notably, the nucleation frequency for filaments originating from the side and ends were decreased by as much as 3-fold in *prf1* mutants,

whereas de novo nucleation of actin filaments increased slightly compared with wild type (Fig. 4C). Collectively, our data demonstrate that PRF1 contributes to nucleation by promoting initiation of filaments that grow from the side of other filaments or bundles in plant cells.

PRF1 Contributes to Actin Stochastic Dynamics by Regulating the Elongation Rate of Different Populations of Actin Filaments

To better understand how PRF1 affects the dynamics of single actin filaments in live cells, several parameters related to actin filament turnover were measured in epidermal cells from the base of 5-d-old dark-grown *prf1* mutant hypocotyls (Staiger et al., 2009; Henty et al., 2011; Li et al., 2012, 2014b). As shown in Table I, not all parameters of single actin filament turnover were affected: severing frequency, regrowth of severed ends, and filament-filament annealing were unchanged in *prf1* mutants compared to wild type. Notably, compared to wild-type siblings (Fig. 5A; Table I), single actin filament elongation rates in the *prf1* mutants were decreased up to 26% and maximum filament length was decreased up to 16% (Fig. 5A; Table I). For maximum filament lifetime, compared to wild type, the value was increased in the *prf1-2* mutant, whereas it was not significantly different in the *prf1-3* mutant (Table I).

Our quantitative analyses demonstrate that actin filament elongation rates were significantly decreased in *prf1* mutants (Fig. 5B). We hypothesize that PRF1 may contribute to actin filament turnover by supporting the growth of distinct populations of filament ends. We categorized actin filament elongation rates into three populations—more than 2 $\mu\text{m/s}$, between 1 and 2 $\mu\text{m/s}$, and less than 1 $\mu\text{m/s}$ —as described previously for budding yeast and plant cells (Yu et al., 2011; Cai et al., 2014; Li et al., 2014b). In wild-type cells, 49% of actin filaments grow at rates between 1 and 2 $\mu\text{m/s}$, only 16% elongate less than 1 $\mu\text{m/s}$, and 35% elongate at more than 2 $\mu\text{m/s}$ (Fig. 5C). In *prf1-2* mutants, most actin filaments still elongate at a rate between 1 and 2 $\mu\text{m/s}$. However, the population of actin filaments elongating at rates less than 1 $\mu\text{m/s}$ was significantly increased to 37%, whereas the population of more than

2 $\mu\text{m/s}$ was decreased to 13%. Similar changes were observed in *prf1-3* cells. Collectively, these data indicate that PRF1 contributes to actin filament dynamics by favoring fast actin filament elongation in Arabidopsis cells.

Inhibition of Formin Activity Leads to Reduced Actin Nucleation and Filament Assembly

The above results imply that PRF1 facilitates actin nucleation from the side of preexisting filaments and supports fast filament assembly in hypocotyl epidermal cells. However, profilin is not a direct actin filament nucleator in cells. The ARP2/3 complex and formins are reported nucleators in plants (Blanchoin et al., 2000). Notably, formins contain a Pro-rich domain (FH1), which allows their association with profilin or profilin-bound actin monomers (Evangelista et al., 1997; Blanchoin et al., 2000; Goode and Eck, 2007). We hypothesize that reduction of formin activity in Arabidopsis would result in decreased nucleation frequency in cells and, further, that this would mimic the *prf* mutant phenotype. To test this, we employed a small molecule inhibitor of formin FH2 domain (SMIFH2), which decreases yeast and mammalian formin-mediated nucleation and elongation in vitro (Rizvi et al., 2009; Rizvi et al., 2009). Although this compound has been applied to plant cells previously and reportedly effects actin filament dynamics (Rosero et al., 2013), we sought to validate its ability to inhibit plant formins in vitro. Using the minimal nucleation domain of Arabidopsis FORMIN1 (AtFORMIN1-FH2D; Michelot et al., 2005), we demonstrated that SMIFH2 could potentially inhibit actin nucleation and assembly in pyrene-actin polymerization assays (Supplemental Fig. S4).

To test the effects of SMIFH2 in the Arabidopsis dark-grown hypocotyl, we applied a dose series of formin inhibitor (0, 1, 10, 25, 50, and 100 μM) for 5 min. Snapshots and time-lapse movies of epidermal cells from the base of 5-d-old dark-grown hypocotyls treated with SMIFH2 were collected by VAEM. The formin inhibitor had a dose-dependent effect on actin array architecture, with concentrations above 10 μM resulting in significantly reduced filament array densities (Supplemental Fig. S5, A and B). The extent of bundling was largely

Table I. Single actin filament dynamics in wild type and *prf1* mutants

Measurements were taken from the basal region of 5-d-old dark-grown hypocotyls. Values represent mean \pm SE. $n \geq 50$ filaments from at least 10 hypocotyls per genotype. ** $P < 0.005$, *** $P < 0.001$, ND $P \geq 0.05$, Student's *t* test.

Stochastic Dynamic Parameters	Wild Type	<i>prf1-2</i>	Wild Type	<i>prf1-3</i>
Elongation rate; $\mu\text{m/s}$	1.72 \pm 0.04	1.39 \pm 0.04***	1.71 \pm 0.09	1.27 \pm 0.07***
Severing frequency; breaks/ $\mu\text{m/s}$	0.017 \pm 0.001	0.017 \pm 0.002 ND	0.011 \pm 0.001	0.010 \pm 0.001 ND
Maximum filament length; μm	12.4 \pm 0.4	11.6 \pm 0.4**	11.3 \pm 0.5	9.8 \pm 0.4**
Maximum filament lifetime; s	20.7 \pm 1.1	24.4 \pm 1.6**	30.2 \pm 1.3	31.4 \pm 1.7 ND
Convoluteness	1.41 \pm 0.07	1.31 \pm 0.05 ND	1.55 \pm 0.09	1.39 \pm 0.09 ND
Rate of convoluteness change; s^{-1}	0.11 \pm 0.01	0.12 \pm 0.02 ND	0.12 \pm 0.03	0.12 \pm 0.03 ND
Regrowth of severed ends; %	2.3 \pm 0.5	1.4 \pm 0.3 ND	2.2 \pm 2.2	3.8 \pm 2.7 ND
Annealing of severed ends; %	2.2 \pm 0.5	2.2 \pm 0.5 ND	2.1 \pm 2.1	3.7 \pm 2.6 ND

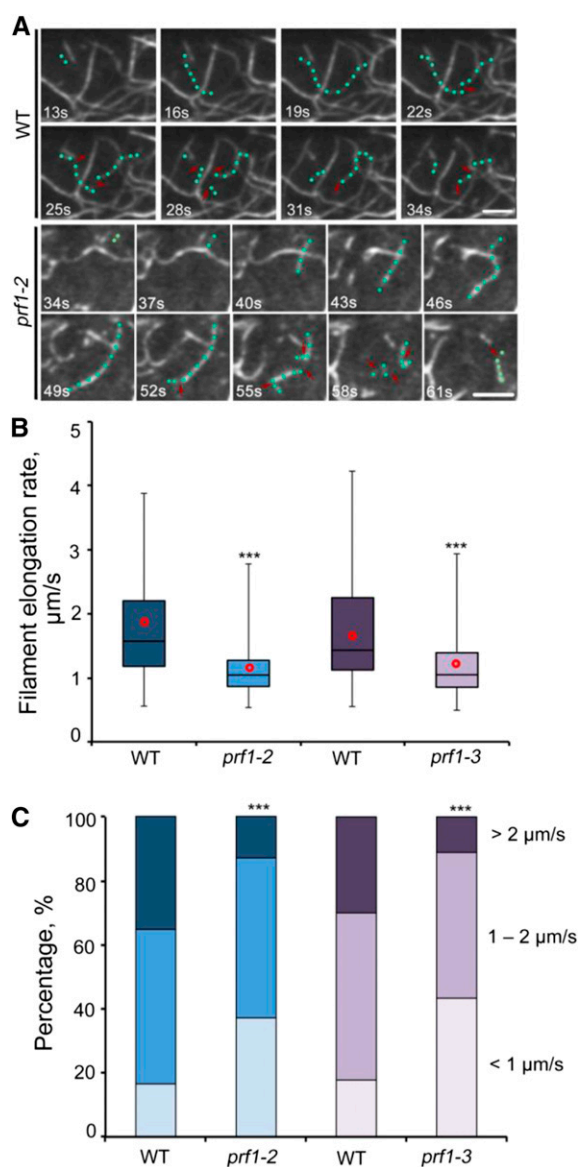


Figure 5. The proportion of filament ends with different elongation rates changes in *prf1* mutants. **A**, A representative actin filament from a wild-type (top) epidermal cell (green dots) elongated rapidly ($1.61 \mu\text{m/s}$) and was subsequently disassembled by numerous severing events (red arrows). A representative actin filament from a *prf1-2* mutant (bottom) epidermal cell elongated more slowly ($0.74 \mu\text{m/s}$) and persisted for a longer period before severing events occurred (red arrows). Bars, $5 \mu\text{m}$. **B**, Box plots show the average filament elongation rate in epidermal cells from 5-d-old etiolated hypocotyls of *prf1-2* and *prf1-3*. The box spans first and third quartiles. The line inside the box shows median value. Bars on the top and bottom represent the maximum and minimum value. The red circles represent mean values for single filament elongation rate. Compared to wild type, the filament elongation rates were significantly slower in *prf1-2* and *prf1-3*. $n \geq 100$ single actin filaments per genotype, $***P < 0.001$, Student's *t* test. **C**, Filament elongation rates were categorized into three populations: more than $2 \mu\text{m/s}$, between 1 and $2 \mu\text{m/s}$, and less than $1 \mu\text{m/s}$, as described previously (Li et al., 2014b). Compared to wild type, the percentage of filament elongation rates $> 2 \mu\text{m/s}$ decreased in *prf1-2* and *prf1-3*, whereas the percentage of filament elongation rates $< 1 \mu\text{m/s}$ increased. $n \geq 100$ single actin filaments per genotype or treatment, $***P < 0.001$, χ^2 test.

unaffected, however, except at the highest concentration of $50 \mu\text{M}$, which resulted in a slight increase in skewness value (Supplemental Fig. S5C)

To address whether filament nucleation was altered, we analyzed the overall nucleation frequency as described above. We found that nucleation frequency was decreased after SMIFH2 treatment of wild-type cells, but a significant decrease occurred only at concentrations greater than $25 \mu\text{M}$ (Fig. 6A). Compared to mock-treated cells (0.62 ± 0.03 events/filament/min), the overall actin nucleation frequency in cells after a 5 min, $25 \mu\text{M}$ SMIFH2 treatment (0.47 ± 0.03 events/filament/min) was significantly decreased (Fig. 6A). Moreover, compared to mock treatment, the frequency of nucleation from the side showed a 40% decrease, and the end of filaments had a 28% decrease after $25 \mu\text{M}$ SMIFH2 treatment, whereas de novo nucleation frequency was only slightly altered (Fig. 6B). Similar changes were observed at other concentrations of SMIFH2 in a dose-dependent manner (Fig. 6B). These observations confirm that formin promotes side nucleation events in plant epidermal cells. Further, the change of nucleation with SMIFH2 treatment phenocopies the *prf1* mutant cells. To test whether formin and profilin might cooperate to execute nucleation of actin filaments in plant cells, we treated the *prf1-2* mutant with $25 \mu\text{M}$ SMIFH2 and evaluated nucleation frequency. The mutant cells were insensitive to SMIFH2 treatment and showed no further reduction in overall nucleation frequency or side-branch formation (Supplemental Fig. S6). This supports the hypothesis that PRF1 and formins function together to regulate actin filament nucleation in plant cells.

Studies in yeast and mammalian cells indicate that profilin promotes formin-mediated processive actin assembly at filament ends (Kovar, 2006). Therefore, we hypothesized that inhibition of formin activity would result in slower actin filament elongation rates. To address this, we measured the elongation rate of single actin filaments after a 5-min SMIFH2 treatment of wild-type epidermal cells. Compared to mock treatment, the elongation rate of growing actin filaments showed a 22% decrease with $25 \mu\text{M}$ SMIFH2 (Fig. 6C). By binning assembling actin filaments into different populations, as we did for *prf1* mutants, we found that the proportion of actin filaments that elongate at rates of more than $2 \mu\text{m/s}$ significantly decreased compared to mock treatment, whereas the population of actin filaments elongating at less than $2 \mu\text{m/s}$ significantly increased (Fig. 6D). Collectively, our data support the view that formin promotes actin assembly in cells and favors the population of actin filaments that elongate at rates greater than $2 \mu\text{m/s}$.

DISCUSSION

In this study, we characterized the function of PRF1 with respect to the regulation of actin dynamics and organization in living cells of Arabidopsis. We found

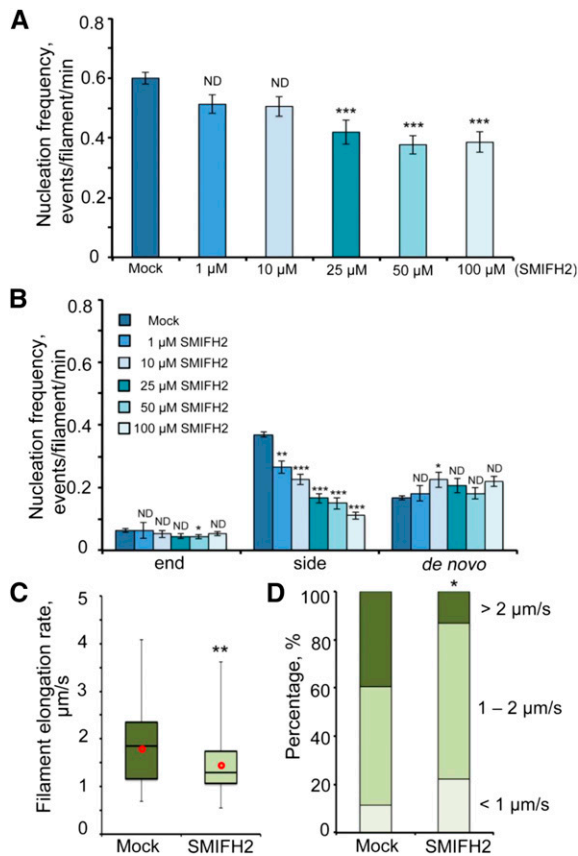


Figure 6. Nucleation frequency and rate of actin filament elongation are inhibited by SMIFH2. A, Nucleation frequency was measured by counting the total nucleation events per filament in a $400 \mu\text{m}^2$ ROI over a 100 s time period after SMIFH2 treatment. Total nucleation frequency was inhibited by SMIFH2 treatment in a dose-dependent manner. Significant decrease of nucleation frequency appeared at concentrations of SMIFH2 greater than $25 \mu\text{M}$. $n > 300$ events from 30 cells of 15 hypocotyls per treatment, Student's t test, $***P < 0.001$. B, Nucleation frequency by origins was analyzed in the same way as described for nucleation frequency in A. Compared to mock treatment, nucleation frequency of filaments originating from the side of a filament or bundle decreased significantly after SMIFH2 treatment. However, nucleation frequency of filaments originating de novo or from ends changed slightly. $n > 300$ events from 30 cells of 15 hypocotyls per treatment, Student's t test, $***P < 0.001$, $**P < 0.01$, $*P < 0.05$, ND $P \geq 0.05$. C, Box plots show the average filament elongation rate in epidermal cells from 5-d-old etiolated hypocotyls without or with a 5 min, $25 \mu\text{M}$ SMIFH2 treatment. The box spans first and third quartiles. The line inside the box shows median value. Bars on the top and bottom represent the maximum and minimum values. The red circles represent mean values for single filament elongation rate. Compared to the mock, the filament elongation rates were significantly slower with SMIFH2 treatment. $n \geq 100$ single actin filaments per treatment, $**P < 0.005$, Student's t test. D, The proportion of single actin filament elongation rates was altered with SMIFH2 treatment. Filament elongation rates were categorized into three populations: more than $2 \mu\text{m/s}$, between 1 and $2 \mu\text{m/s}$, and less than $1 \mu\text{m/s}$, as described previously (Li et al., 2014b). Compared to mock treatment, the percentage of filament elongation rates $> 2 \mu\text{m/s}$ decreased with SMIFH2 treatment, whereas the percentage of filament elongation rates $< 1 \mu\text{m/s}$ increased. $n \geq 100$ single actin filaments per treatment, $*P < 0.05$, χ^2 test.

that axial cell expansion was enhanced when PRF1 protein level is decreased in etiolated hypocotyl epidermal cells and in light-grown root cells. This correlated with altered cytoskeletal architecture in *prf1* mutant cells. Interestingly, we observed that filament nucleation frequency was significantly decreased in *prf1* mutants. Moreover, we found that PRF1 supports high actin filament elongation rates; specifically, it is involved in the growth of a subpopulation of filaments that extend at rates more than $2 \mu\text{m/s}$. Other properties, such as maximum filament length and maximum filament lifetime, were also affected in *prf1* mutants. These results are, to our knowledge, the first genetic evidence for regulation of actin dynamics by PRF1 and demonstrate a requirement for plant profilin to facilitate the nucleation and assembly of actin filaments.

PRF1 Participates in the Regulation of Actin Filament Stochastic Dynamics in Living Cells of Arabidopsis

We characterized two Arabidopsis T-DNA insertion lines in which PRF1 protein levels were significantly reduced. The density of actin filament arrays was significantly decreased in *prf1* cells from several tissues. This is somewhat hard to interpret based on the biochemical properties of profilin and actin in vitro. Several mechanisms are thought to maintain the abundance of actin filaments in cells: the ratio of monomeric to F-actin, actin nucleation frequency, filament polymerization rates, and the availability of filament ends (Pollard et al., 2000). It is noteworthy that the 10:1 ratio of monomeric to F-actin is much higher in plant cells than in animal and yeast systems (Wang et al., 2005; Staiger and Blanchoin, 2006). Profilin is considered to have multifaceted effects on the assembly of actin filaments depending on the availability of barbed ends. When the barbed end is uncapped, profilin promotes actin filament elongation, whereas ADP-actin monomer depolymerizes from pointed ends when the barbed end is occupied with capping protein (CP; Sun et al., 1995; Staiger et al., 1997; Pollard et al., 2000). Therefore, the status of actin filament barbed ends might be a potential mechanism for the function of PRF1 on the polymerization of actin filaments in vivo.

Previously, we established metrics to describe the dynamic properties of single actin filaments from time-lapse VAEM images, including filament elongation rate, severing frequency, maximum filament length, and maximum filament lifetime (Staiger et al., 2009; Henty et al., 2011; Li et al., 2012; Henty-Ridilla et al., 2013; Li et al., 2014b). By analyzing these parameters in live epidermal cells, we demonstrated that ADF4 facilitates the turnover of actin filaments through its severing activity (Henty et al., 2011) and that CP regulates filament ends to contribute to the remodeling of actin filaments (Li et al., 2012, 2014b). In this study, reduction of PRF1 protein levels led to a significant decrease in actin filament elongation rate and maximum filament length but, in contrast, increased the maximum filament lifetime. These data provide

compelling evidence that profilin promotes the polymerization of actin filaments at barbed ends *in vivo*. Similar results were reported recently for a *prf4 prf5* double mutant of Arabidopsis; specifically, F-actin content and filament elongation rates were reduced when profilin levels are decreased in pollen (Liu et al., 2015). Elongation of actin filaments is determined by two factors: regulation of actin monomers and the availability of filament ends (Pollard et al., 2000). It has been suggested that profilin facilitates filament assembly by boosting nucleotide exchange on actin monomers (Wolven et al., 2000; Lu and Pollard, 2001); however, plant profilins do not have this activity or actually inhibit nucleotide exchange on plant actin (Perelroizen et al., 1996; Kovar et al., 2001). In Arabidopsis, adenylyl cyclase-associated protein (CAP) is able to mediate nucleotide exchange on G-actin *in vitro* (Chaudhry et al., 2007). One possible mechanism suggests that PRF1 functions synergistically with CAP in Arabidopsis to regulate actin filament growth at barbed ends. Indeed, the cooperation between plant ADF, CAP, and profilin has been demonstrated to facilitate the recycling of ADP-actin and treadmilling through the filament pool *in vitro* (Chaudhry et al., 2007). Since single actin filaments do not exhibit treadmilling behavior *in vivo* (Staiger et al., 2009), additional mechanisms for profilin function must be considered.

PRF1 Is Implicated in FORMIN-Mediated Actin Nucleation and Filament Elongation

Previous biochemical data indicate that plant profilin suppresses spontaneous nucleation from a pool of monomers *in vitro* (Michelot et al., 2005; Staiger and Blanchoin, 2006). Based on this, we hypothesized that filament nucleation frequency would be increased in *prf1* mutants, because of the presumed greater availability of free monomers. However, the results were the exact opposite; *prf1* mutants had a significantly reduced overall actin nucleation frequency. Our interpretation is that the function of PRF1 on actin nucleation in plant cells is not limited to spontaneous nucleation or, conversely, PRF1 is necessary for the function of specific nucleators in plant cells. Two important types of actin nucleators in eukaryotic cells are ARP2/3 complex and formin (Pollard et al., 2000; Pruyne et al., 2002). The ARP2/3 complex nucleates actin filaments preferentially associated with the side of preexisting filaments *in vitro*. Furthermore, the ARP2/3 complex remains bound to the pointed end of growing actin filaments, whereas the free barbed ends are quickly occupied by CP. The ARP2/3 complex contributes to the formation of dendritic actin filament arrays and favors network formation in mammalian cells but its molecular mechanism in plants is poorly defined (Blanchoin et al., 2000).

Formin bears a conserved actin-binding domain, formin-homology 2 (FH2), and a Pro-rich domain, formin-homology 1 (FH1), which binds to profilin or

profilin-bound actin monomers efficiently (Evangelista et al., 1997; Blanchoin et al., 2000; Goode and Eck, 2007). Budding yeast formins nucleate and stimulate the assembly of unbranched filaments *in vitro* (Pruyne et al., 2002) and contribute to the formation of actin cables *in vivo* (Evangelista et al., 1997). Studies in both animal and yeast cells demonstrate that several formins processively associate with barbed ends to facilitate the creation of long actin filaments from profilin-actin (Kovar and Pollard, 2004; Romero et al., 2004; Kovar, 2006). Recent studies in fission yeast and mammalian systems show that profilin functions as a gatekeeper for the allocation of actin monomers to ARP2/3- or formin-dependent pathways (Suarez et al., 2015; Rotty et al., 2015). Through single-molecule imaging techniques *in vitro*, profilin-bound actin monomers were observed to favor formin-mediated long, unbranched actin filament formation and inhibit ARP2/3-mediated short, branched actin networks. Our data demonstrate directly that PRF1 is involved in both filament nucleation and elongation in plant cells.

PRF1 is probably a key element in the formin-mediated nucleation process in Arabidopsis. More than 20 Arabidopsis FORMIN isovariants exist (Blanchoin and Michelot, 2012; Cvrčková, 2013). FORMIN1 (AtFH1) promotes actin polymerization more efficiently from a pool of profilin-bound actin monomers than from free actin monomers *in vitro* (Michelot et al., 2005). However, AtFH1 is a nonprocessive nucleator that binds to the side of preexisting actin filaments and nucleates branched filament assembly (Michelot et al., 2006). In this study, we observed that the population of nucleation events that originates from the side of a mother filament was significantly decreased in *prf1* mutants, which indicates that PRF1 favors the formation of side/branched filament creation. Based on the observation that SMIFH2 treatment recapitulates the *prf1* phenotype of reduced side nucleation, it seems likely that PRF1 cooperates with AtFH1, and perhaps other formins, to regulate branched actin filament formation in plant cells.

Further genetic analyses should be designed to dissect the interaction between formin and profilin in Arabidopsis. Overexpression of AtFH1 in pollen tubes promotes the formation of actin bundles (Cheung and Wu, 2004; Cheung et al., 2010). However, a recent report on *Arabidopsis fhl1* T-DNA insertion mutants showed the presence of more bundles compared to wild-type rhizodermis cells (Rosero et al., 2013). Unfortunately, single filament properties, like nucleation frequency and elongation rate, were not analyzed in the *fhl1* mutants. Future work with the *fhl1* mutants should test whether those metrics are affected. If PRF1 and AtFH1 cooperate, we expect both reduced elongation rate and nucleation frequency of branched filaments in the *fhl1* mutants.

In addition to nucleation, most formins bind to the barbed end of actin filaments and facilitate filament elongation in a processive manner (Kovar and Pollard, 2004). Evidence from yeast and animal systems indicate

that formin-mediated actin filament elongation rates increase 5- to 10-fold in the presence of profilin and promote the formation of long cables/filaments (Kovar and Pollard, 2004; Romero et al., 2004; Kovar, 2006). The same is true of For2, a type II formin from *P. patens* (Vidali et al., 2009). Direct evidence came from the visualization of actin elongation by the FH1-FH2 domains of For2 protein in vitro. Although the FH1 domain of For2 is rich in contiguous Pro repeats, actin elongation activity was lower in the presence of human profilin (Vidali et al., 2009; van Gisbergen and Bezanilla, 2013). In Arabidopsis, AtFH1 is capable of promoting actin nucleation but is a nonprocessive formin in vitro that leaves filament barbed ends free for assembly or capping by CP (Michelot et al., 2005; Michelot et al., 2006). According to previous reports on budding yeast cells, distinct subpopulations of cable elongation rates are driven by different mechanisms (Chesarone-Cataldo et al., 2011; Yu et al., 2011). For example, the subpopulation of filaments that elongate at rates of 1 to 2 $\mu\text{m/s}$ depends on the formins Bni1 and Bnr1.

To test whether different subpopulations of growing actin filaments exist in plant cells, we categorized growing filament rates into three populations, as described for budding yeast, and analyzed the percentage of different actin filament elongation rates in *cpb-1* mutants and *CPOX#1* seedlings (Li et al., 2014b). We demonstrate that excess CP prefers to bind the barbed ends of filaments that grow at rates of more than 2 $\mu\text{m/s}$ (Li et al., 2014b). Similarly, we addressed the question whether PRF1 affects the distribution of a subpopulation of actin filament elongation rates in plant cells. In *prf1* mutants, average filament elongation rates were significantly decreased. These data indicate that PRF1 favors a subpopulation of fast-growing filaments that elongate at rates of more than 2 $\mu\text{m/s}$ and also support our previous hypothesis that growing filament barbed ends in plant cells are either free or bound by formin (Li et al., 2014a). Although evidence in vitro shows that AtFH1 is a nonprocessive formin (Michelot et al., 2006), we should not exclude the possibility that processive FORMINs exist in Arabidopsis. If other formin isoforms are processive elongation factors, we expect a reduction of the fast-growing filament population in specific *formin* mutants.

PRF1 Is Involved in the Modulation of Cell Expansion and Morphogenesis

The mechanism that coordinates cell expansion with actin cytoskeleton organization is a long-standing-but-unresolved question for plant cell biologists (Smith and Oppenheimer, 2005; Hussey et al., 2006; Szymanski and Cosgrove, 2009). It is a generally held view that the cortical actin cytoskeleton affects anisotropic cell expansion by providing long tracks for the delivery of cell wall materials to the growth sites (Smith and Oppenheimer, 2005; Sampathkumar et al., 2013; Li et al., 2014a). Perturbing the actin cytoskeleton with

actin-disrupting drugs (cytochalasin and latrunculin) impairs Golgi-derived vesicle secretion and inhibits directed tip growth (Hepler et al., 2001). Moreover, accumulating evidence from actin or ABP deficient mutants indicates that disturbance of the actin cytoskeleton leads to obvious defects in cell expansion and morphogenesis (Dyachok et al., 2011; Henty et al., 2011; Li et al., 2012; Cai et al., 2014; Li et al., 2014b).

Profilin is reported to affect plant cell expansion in several studies. For example, tip growth in moss protonemal cells is inhibited in *profilin* RNAi mutants (Vidali et al., 2010). In Arabidopsis, Ramachandran et al. (2000) generated *profilin* overexpression (PFN-O) and underexpression (PFN-U) plants. They observed dwarf and shorter etiolated hypocotyls and roots in PFN-U seedlings (Ramachandran et al., 2000). In contrast, Meagher's group found that the *prf1-1* mutant, which contains a T-DNA insertion in the promoter region of the *PRF1* gene, has longer dark-grown hypocotyls and elevated organs (McKinney et al., 2001). Interestingly, another T-DNA insertion mutant in the first intron of *PRF1* gene, *prf1-4*, results in light-grown seedlings and plants with a modest dwarfed phenotype (Müssar et al., 2015). These observations indicate that defects of *PRF1* in Arabidopsis disrupt normal cell expansion and morphogenesis. Here, we used two T-DNA insertion mutants, *prf1-2* and *prf1-3*, and observed that reduction of PRF1 levels in plants resulted in longer hypocotyl and root epidermal cells. Our data support the idea that PRF1 is involved in the axial cell expansion process. However, the molecular mechanism that underpins how the actin cytoskeleton in *prf1* mutants regulates cell expansion is unclear.

To address the role of actin cytoskeleton during cell growth, we previously analyzed axial cell expansion in several ABP mutants with opposite effects on actin architecture in cells but discovered that there was no direct correlation between the organization of actin arrays and cell expansion (Henty et al., 2011; Li et al., 2012; Cai et al., 2014). However, two single-filament parameters, maximum actin filament length and lifetime, were found to positively correlate with axial cell expansion. It is predicted that increased filament length and lifetime could provide longer and more stable tracks for vesicle trafficking to expansion sites where exocytosis occurs and thereby promote cell growth (Li et al., 2014a, 2014b, 2015). In *prf1* mutants, the lifetime of single actin filaments was increased, which supports this model and explains the increased hypocotyl cell elongation; however, the modestly reduced filament length in *prf1* mutants challenges this interpretation.

It is noteworthy that there are several additional factors in plants to organize cell expansion and polarity establishment. For example, the Rho GTPase of Plant (ROP) signaling pathway has been reported to guide polarity establishment of the puzzle-piece-shaped epidermal pavement cells in Arabidopsis leaves. The ROP2-RIC4 pathway promotes the formation of dynamic actin filaments in the lobe region and supports the local protrusion of pavement cells (Fu et al., 2005).

Recently, Yang's group demonstrated that the ROP2-RIC4 pathway regulates local endocytosis of PIN1 protein, an auxin transporter, to facilitate lobe formation in pavement cells (Nagawa et al., 2012). This provides us a broad view to explore the correlation between actin cytoskeleton and cell expansion. Future work should address the properties of vesicle trafficking and PIN polarity in actin-deficient mutants during cell morphogenesis.

MATERIALS AND METHODS

Plant Material and Growth Conditions

Arabidopsis (*Arabidopsis thaliana*) ecotype Columbia-0 was used in this study. Two *PRF1* T-DNA insertion lines, *prf1-2* (SALK_057718) and *prf1-3* (SALK_143800), and a *PRF2* T-DNA insertion line, *prf2* (SALK_129071), obtained from the Arabidopsis Biological Resource Center (The Ohio State University), were crossed to wild-type Columbia-0 expressing the GFP-fABD2 reporter (Sheahan et al., 2004; Staiger et al., 2009). Homozygous mutants, as well as wild-type siblings, were recovered from F2 populations. Individuals were genotyped by PCR using primers described in Supplemental Table S1. Homozygous F3 or F4 plants expressing GFP-fABD2 were used for all experiments.

Seeds were surface-sterilized with a solution of 50% (v/v) bleach and 0.1% (w/v) SDS, plated on half-strength Murashige and Skoog medium supplemented with 1% (w/v) agar and 1% (w/v) Suc, and kept at 4°C for 48 h before transfer to the growth chamber. After exposure to light for 2 h, plates were covered with foil and grown at 21°C for 5 d before imaging of hypocotyl epidermal cells. For root growth analysis, seed was sown on plates prepared with half-strength Murashige and Skoog medium supplemented with 0.6% (w/v) agar without Suc and grown vertically under long day conditions (16 h light/8 h dark).

A double-blind experimental design was used for all phenotypic analyses. All image measurements were performed with Image J (<http://rsb.info.nih.gov/ij/>).

RNA Extraction and qRT-PCR

Total RNA was extracted from 7-d-old dark-grown hypocotyls. Seedlings were transferred to liquid nitrogen immediately after harvest and ground into a powder with precooled pestles. TRIzol reagent (Invitrogen) was used for RNA purification, according to the manufacturer's protocol. RNA was reverse-transcribed using SuperScript II Reverse Transcriptase (Invitrogen) and Random Primer Mix (New England Biolabs). To determine *PRF1* expression levels in hypocotyls, qRT-PCR was performed using FastStart SYBR Green master mix and a LightCycler 96 thermocycler (Roche). Primers for *PRF1* are shown in Supplemental Table S1. For all experiments, gene expression was normalized to *GAPD* transcript levels (Khurana et al., 2010; Henty et al., 2011; Li et al., 2012). Three biological and technical repeats were performed for each genotype.

Semiquantitative Immunoblotting

Five-day-old dark-grown seedlings of *prf1-2 GFP-fABD2*, *prf1-3 GFP-fABD2*, *prf2 GFP-fABD2*, and corresponding wild-type siblings were used to estimate PRF1 protein levels. About 0.2 g of whole-plant material was ground with liquid nitrogen into a fine powder and suspended with homogenization buffer containing 20 mM HEPES/KCl, pH 7.2, 50 mM KOAc, 2 mM Mg(OAc)₂, 250 mM sorbitol, 1 mM EDTA, 1 mM EGTA, 1 mM DTT, 1 mM PMSF, and 1% (v/v) protease inhibitor cocktail (2 mM *o*-phenanthroline, 0.5 mg/mL leupeptin, 2 mg/mL aprotinin, 1 mg/mL pepstatin). This was followed by centrifugation at 4°C, 15,000g for 5 min, as described previously (Chaudhry et al., 2007). Total protein concentration from supernatant was determined with the Bradford assay (Protein Assay; Bio-Rad) using bovine serum albumin as a standard. For each genotype, 4 μg of total protein was loaded on the same SDS-PAGE. Proteins separated by SDS-PAGE were transferred to nitrocellulose membranes and probed with anti-PRF1a antibodies (Kerafast) at a dilution of 1:2000, as described by McKinney et al. (2001). Actin was detected on the same membranes using the JLA-20 monoclonal antibody (Developmental Studies

Hybridoma Bank, University of Iowa). Phosphoenolpyruvate carboxylase antibody (Rockland Immunochemicals) was used as a loading control. The blots were incubated in horseradish peroxidase-coupled secondary antibody (Sigma-Aldrich) at 1:50,000 dilution and developed with SuperSignal Pico West chemiluminescent substrate (Thermo Scientific) according to manufacturer's instructions. Densitometric analysis was performed for quantitative measurements of protein levels using ImageJ. Fold change in PRF1 level, normalized to phosphoenolpyruvate carboxylase antibody and relative to protein levels in the control sample, was calculated. Five biological replicates were performed per genotype.

Time-Lapse Imaging of Actin Filament Dynamics

Fluorescent images of epidermal cells were collected using time-lapse VAEM as described previously (Staiger et al., 2009; Henty et al., 2011; Li et al., 2012). An Olympus TIRF objective (60×, 1.45 numerical aperture) was used. Images were acquired using SlideBook software (version 5.5; Intelligent Imaging Innovations) and processed with Image J or Photoshop software (Adobe Systems).

The cortical actin cytoskeleton in epidermal cells was imaged in 5-d-old dark-grown hypocotyls expressing GFP-fABD2 (Staiger et al., 2009). To compare single actin filament parameters between *prf1* mutant and wild-type sibling cells, double-blind experiments (data collection and analysis) were performed. Maximum filament length and lifetime, filament severing frequency, and elongation rates were measured as described previously (Staiger et al., 2009; Henty et al., 2011; Li et al., 2012, 2014b). Regrowth or annealing frequency of the presumed plus ends was determined as a percentage; the number of events observed was divided by the total number of ends for each growing filament and multiplied by 100. For nucleation frequency analysis, a 400 μm² ROI was randomly selected from images of epidermal cells at the base of the hypocotyl, and all observable nucleation events were counted during a 100 s time period. For this parameter, more than 380 events from 15 hypocotyls were observed per genotype. To account for differences in filament density in genotypes, nucleation frequency was normalized against filament numbers in the ROI.

Quantitative Analyses of Cytoskeleton Architecture

To quantify actin architecture, two parameters, skewness and density, were employed in this study; these parameters describe the extent of actin filament bundling and the percentage of occupancy of GFP signal in an image, respectively, as noted previously (Higaki et al., 2010; Khurana et al., 2010; Henty et al., 2011; Li et al., 2012). All images used for these parameters were collected with a fixed exposure time, laser power, and camera gain setting for *prf1* mutants and their respective controls. Micrographs were analyzed in Image J using the methods described previously (Higaki et al., 2010; Henty et al., 2011; Li et al., 2012). For these measurements, at least 300 images of hypocotyl epidermal cells per genotype or more than 236 images of epidermal cells from root elongation zone were collected from 15 individual seedlings per genotype.

Sequence data for *PRF1* can be found in the Arabidopsis Genome Initiative database (accession no. AT2G19760).

Supplemental Data

The following supplemental materials are available.

Supplemental Figure S1. The average pixel intensity of single actin filaments is not altered in the *prf1* mutants.

Supplemental Figure S2. Phalloidin labeling of actin array architecture gives similar results to live-cell imaging of GFP-fABD2.

Supplemental Figure S3. PRF1 is required for actin organization in epidermal cells of the cotyledon in Arabidopsis.

Supplemental Figure S4. AtFormin1-mediated actin nucleation is inhibited by SMIFH2 in vitro

Supplemental Figure S5. The density of actin filament arrays is reduced following treatment with SMIFH2.

Supplemental Figure S6. The frequency of filament nucleation in *prf1-2* mutant is insensitive to SMIFH2 treatment.

Supplemental Table S1. Primers used for genotyping and qRT-PCR.

ACKNOWLEDGMENTS

We thank Hongbing Luo (Purdue University) for excellent care and maintenance of plant material, Christophe Guerin (Institut de Recherches en Technologie et Sciences pour le Vivant, Grenoble) for performing pyrene-actin assembly assays, and Drs. David Kovar and Cristian Suarez (University of Chicago) for helpful comments. We are also grateful to the Arabidopsis Biological Resource Center at The Ohio State University for supplying T-DNA insertion lines. The TIRF microscopy facility was supported, in part, by the Bindley Bioscience Center at Purdue.

Received August 20, 2015; accepted November 16, 2015; published November 16, 2015.

LITERATURE CITED

- Baskin TI (2005) Anisotropic expansion of the plant cell wall. *Annu Rev Cell Dev Biol* **21**: 203–222
- Blanchoin L, Amann KJ, Higgs HN, Marchand JB, Kaiser DA, Pollard TD (2000) Direct observation of dendritic actin filament networks nucleated by Arp2/3 complex and WASP/Scar proteins. *Nature* **404**: 1007–1011
- Blanchoin L, Boujemaa-Paterski R, Henty JL, Khurana P, Staiger CJ (2010) Actin dynamics in plant cells: a team effort from multiple proteins orchestrates this very fast-paced game. *Curr Opin Plant Biol* **13**: 714–723
- Blanchoin L, Boujemaa-Paterski R, Sykes C, Plastino J (2014) Actin dynamics, architecture, and mechanics in cell motility. *Physiol Rev* **94**: 235–263
- Blanchoin L, Michelot A (2012) Actin cytoskeleton: a team effort during actin assembly. *Curr Biol* **22**: R643–R645
- Cai C, Henty-Ridilla JL, Szymanski DB, Staiger CJ (2014) Arabidopsis myosin XI: a motor rules the tracks. *Plant Physiol* **166**: 1359–1370
- Chaudhry F, Guérin C, von Witsch M, Blanchoin L, Staiger CJ (2007) Identification of *Arabidopsis* cyclase-associated protein 1 as the first nucleotide exchange factor for plant actin. *Mol Biol Cell* **18**: 3002–3014
- Chesarone-Cataldo M, Guérin C, Yu JH, Wedlich-Soldner R, Blanchoin L, Goode BL (2011) The myosin passenger protein Smy1 controls actin cable structure and dynamics by acting as a formin damper. *Dev Cell* **21**: 217–230
- Cheung AY, Niroomand S, Zou Y, Wu HM (2010) A transmembrane formin nucleates subapical actin assembly and controls tip-focused growth in pollen tubes. *Proc Natl Acad Sci USA* **107**: 16390–16395
- Cheung AY, Wu HM (2004) Overexpression of an Arabidopsis formin stimulates supernumerary actin cable formation from pollen tube cell membrane. *Plant Cell* **16**: 257–269
- Christensen HE, Ramachandran S, Tan CT, Surana U, Dong CH, Chua NH (1996) *Arabidopsis* profilins are functionally similar to yeast profilins: identification of a vascular bundle-specific profilin and a pollen-specific profilin. *Plant J* **10**: 269–279
- Cvrčková F (2013) Formins and membranes: anchoring cortical actin to the cell wall and beyond. *Front Plant Sci* **4**: 436
- dos Remedios CG, Chhabra D, Kekic M, Dedova IV, Tsubakihara M, Berry DA, Nosworthy NJ (2003) Actin binding proteins: regulation of cytoskeletal microfilaments. *Physiol Rev* **83**: 433–473
- Dyachok J, Zhu L, Liao F, He J, Huq E, Blancaflor EB (2011) SCAR mediates light-induced root elongation in *Arabidopsis* through photoreceptors and proteasomes. *Plant Cell* **23**: 3610–3626
- Ehrhardt DW, Bezanilla M (2013) Patterning the cell: membrane-cytoskeleton crosstalk. *Curr Opin Plant Biol* **16**: 675–677
- Evangelista M, Blundell K, Longtine MS, Chow CJ, Adames N, Pringle JR, Peter M, Boone C (1997) Bni1p, a yeast formin linking cdc42p and the actin cytoskeleton during polarized morphogenesis. *Science* **276**: 118–122
- Fu Y, Gu Y, Zheng Z, Wasteneys G, Yang Z (2005) *Arabidopsis* interdigitating cell growth requires two antagonistic pathways with opposing action on cell morphogenesis. *Cell* **120**: 687–700
- Gendreau E, Traas J, Desnos T, Grandjean O, Caboche M, Höfte H (1997) Cellular basis of hypocotyl growth in *Arabidopsis thaliana*. *Plant Physiol* **114**: 295–305
- Goode BL, Eck MJ (2007) Mechanism and function of formins in the control of actin assembly. *Annu Rev Biochem* **76**: 593–627
- Henty JL, Bledsoe SW, Khurana P, Meagher RB, Day B, Blanchoin L, Staiger CJ (2011) *Arabidopsis* actin depolymerizing factor4 modulates the stochastic dynamic behavior of actin filaments in the cortical array of epidermal cells. *Plant Cell* **23**: 3711–3726
- Henty-Ridilla JL, Li J, Blanchoin L, Staiger CJ (2013) Actin dynamics in the cortical array of plant cells. *Curr Opin Plant Biol* **16**: 678–687
- Hepler PK, Vidali L, Cheung AY (2001) Polarized cell growth in higher plants. *Annu Rev Cell Dev Biol* **17**: 159–187
- Higaki T, Kutsuna N, Sano T, Kondo N, Hasezawa S (2010) Quantification and cluster analysis of actin cytoskeletal structures in plant cells: role of actin bundling in stomatal movement during diurnal cycles in Arabidopsis guard cells. *Plant J* **61**: 156–165
- Huang S, McDowell JM, Weise MJ, Meagher RB (1996) The Arabidopsis profilin gene family. Evidence for an ancient split between constitutive and pollen-specific profilin genes. *Plant Physiol* **111**: 115–126
- Hussey PJ, Ketelaar T, Deeks MJ (2006) Control of the actin cytoskeleton in plant cell growth. *Annu Rev Plant Biol* **57**: 109–125
- Kandasamy MK, McKinney EC, Meagher RB (2002) Plant profilin isoforms are distinctly regulated in vegetative and reproductive tissues. *Cell Motil Cytoskeleton* **52**: 22–32
- Khurana P, Henty JL, Huang S, Staiger AM, Blanchoin L, Staiger CJ (2010) *Arabidopsis* VILLIN1 and VILLIN3 have overlapping and distinct activities in actin bundle formation and turnover. *Plant Cell* **22**: 2727–2748
- Konopka CA, Bednarek SY (2008) Variable-angle epifluorescence microscopy: a new way to look at protein dynamics in the plant cell cortex. *Plant J* **53**: 186–196
- Kovar DR (2006) Cell polarity: formin on the move. *Curr Biol* **16**: R535–R538
- Kovar DR, Dröbak BK, Staiger CJ (2000) Maize profilin isoforms are functionally distinct. *Plant Cell* **12**: 583–598
- Kovar DR, Dröbak BK, Collings DA, Staiger CJ (2001) The characterization of ligand-specific maize (*Zea mays*) profilin mutants. *Biochem J* **358**: 49–57
- Kovar DR, Kuhn JR, Tichy AL, Pollard TD (2003) The fission yeast cytokinesis formin Cdc12p is a barbed end actin filament capping protein gated by profilin. *J Cell Biol* **161**: 875–887
- Kovar DR, Pollard TD (2004) Progressing actin: formin as a processive elongation machine. *Nat Cell Biol* **6**: 1158–1159
- Li J, Arieti R, Staiger CJ (2014a). Actin filament dynamics and their role in plant cell expansion. *In* H Fukuda, ed, *Plant Cell Wall Patterning and Cell Shape* John Wiley & Sons, New York, NY, pp 127–162
- Li J, Blanchoin L, Staiger CJ (2015) Signaling to actin stochastic dynamics. *Annu Rev Plant Biol* **66**: 415–440
- Li J, Henty-Ridilla JL, Huang S, Wang X, Blanchoin L, Staiger CJ (2012) Capping protein modulates the dynamic behavior of actin filaments in response to phosphatidic acid in *Arabidopsis*. *Plant Cell* **24**: 3742–3754
- Li J, Staiger BH, Henty-Ridilla JL, Abu-Abied M, Sadot E, Blanchoin L, Staiger CJ (2014b) The availability of filament ends modulates actin stochastic dynamics in live plant cells. *Mol Biol Cell* **25**: 1263–1275
- Liu X, Qu X, Jiang Y, Chang M, Zhang R, Wu Y, Fu Y, Huang S (2015) Profilin regulates apical actin polymerization to control polarized pollen tube growth. *Mol Plant* **8**: 1694–1709
- Lu J, Pollard TD (2001) Profilin binding to poly-L-proline and actin monomers along with ability to catalyze actin nucleotide exchange is required for viability of fission yeast. *Mol Biol Cell* **12**: 1161–1175
- Ma L, Sun N, Liu X, Jiao Y, Zhao H, Deng XW (2005) Organ-specific expression of Arabidopsis genome during development. *Plant Physiol* **138**: 80–91
- Machesky LM, Cole NB, Moss B, Pollard TD (1994) Vaccinia virus expresses a novel profilin with a higher affinity for polyphosphoinositides than actin. *Biochemistry* **33**: 10815–10824
- McKinney EC, Kandasamy MK, Meagher RB (2001) Small changes in the regulation of one Arabidopsis profilin isoform, PRF1, alter seedling development. *Plant Cell* **13**: 1179–1191
- Michelot A, Derivery E, Paterski-Boujemaa R, Guérin C, Huang S, Parcy F, Staiger CJ, Blanchoin L (2006) A novel mechanism for the formation of actin-filament bundles by a nonprocessive formin. *Curr Biol* **16**: 1924–1930
- Michelot A, Guérin C, Huang S, Ingouff M, Richard S, Rodiuc N, Staiger CJ, Blanchoin L (2005) The formin homology 1 domain modulates the actin nucleation and bundling activity of Arabidopsis FORMIN1. *Plant Cell* **17**: 2296–2313
- Moseley JB, Goode BL (2005) Differential activities and regulation of *Saccharomyces cerevisiae* formin proteins Bni1 and Bnr1 by Bud6. *J Biol Chem* **280**: 28023–28033
- Müssar KJ, Kandasamy MK, McKinney EC, Meagher RB (2015) Arabidopsis plants deficient in constitutive class profilins reveal independent and quantitative genetic effects. *BMC Plant Biol* **15**: 177

- Nagawa S, Xu T, Lin D, Dhonukshe P, Zhang X, Friml J, Scheres B, Fu Y, Yang Z (2012) ROP GTPase-dependent actin microfilaments promote PIN1 polarization by localized inhibition of clathrin-dependent endocytosis. *PLoS Biol* **10**: e1001299
- Pantaloni D, Carlier MF (1993) How profilin promotes actin filament assembly in the presence of thymosin beta 4. *Cell* **75**: 1007–1014
- Perelroizen I, Didry D, Christensen H, Chua NH, Carlier MF (1996) Role of nucleotide exchange and hydrolysis in the function of profilin in actin assembly. *J Biol Chem* **271**: 12302–12309
- Pleskot R, Li J, Zárský V, Potocký M, Staiger CJ (2013) Regulation of cytoskeletal dynamics by phospholipase D and phosphatidic acid. *Trends Plant Sci* **18**: 496–504
- Pollard TD, Blanchoin L, Mullins RD (2000) Molecular mechanisms controlling actin filament dynamics in nonmuscle cells. *Annu Rev Biophys Biomol Struct* **29**: 545–576
- Pollard TD, Cooper JA (1984) Quantitative analysis of the effect of *Acanthamoeba* profilin on actin filament nucleation and elongation. *Biochemistry* **23**: 6631–6641
- Pruyne D, Evangelista M, Yang C, Bi E, Zigmund S, Bretscher A, Boone C (2002) Role of formins in actin assembly: nucleation and barbed-end association. *Science* **297**: 612–615
- Ramachandran S, Christensen HE, Ishimaru Y, Dong CH, Chao-Ming W, Cleary AL, Chua NH (2000) Profilin plays a role in cell elongation, cell shape maintenance, and flowering in *Arabidopsis*. *Plant Physiol* **124**: 1637–1647
- Rizvi SA, Neidt EM, Cui J, Feiger Z, Skau CT, Gardel ML, Kozmin SA, Kovar DR (2009) Identification and characterization of a small molecule inhibitor of formin-mediated actin assembly. *Chem Biol* **16**: 1158–1168
- Romero S, Le Clainche C, Didry D, Egile C, Pantaloni D, Carlier MF (2004) Formin is a processive motor that requires profilin to accelerate actin assembly and associated ATP hydrolysis. *Cell* **119**: 419–429
- Rosero A, Zárský V, Cvrčková F (2013) AtFH1 formin mutation affects actin filament and microtubule dynamics in *Arabidopsis thaliana*. *J Exp Bot* **64**: 585–597
- Rotty JD, Wu C, Haynes EM, Suarez C, Winkelman JD, Johnson HE, Haugh JM, Kovar DR, Bear JE (2015) Profilin-1 serves as a gatekeeper for actin assembly by Arp2/3-dependent and -independent pathways. *Dev Cell* **32**: 54–67
- Rounds CM, Bezanilla M (2013) Growth mechanisms in tip-growing plant cells. *Annu Rev Plant Biol* **64**: 243–265
- Sampathkumar A, Gutierrez R, McFarlane HE, Bringmann M, Lindeboom J, Emons AM, Samuels L, Ketelaar T, Ehrhardt DW, Persson S (2013) Patterning and lifetime of plasma membrane-localized cellulose synthase is dependent on actin organization in *Arabidopsis* interphase cells. *Plant Physiol* **162**: 675–688
- Sheahan MB, Staiger CJ, Rose RJ, McCurdy DW (2004) A green fluorescent protein fusion to actin-binding domain 2 of *Arabidopsis* fimbrin highlights new features of a dynamic actin cytoskeleton in live plant cells. *Plant Physiol* **136**: 3968–3978
- Smertenko AP, Deeks MJ, Hussey PJ (2010) Strategies of actin re-organisation in plant cells. *J Cell Sci* **123**: 3019–3028
- Smith LG, Oppenheimer DG (2005) Spatial control of cell expansion by the plant cytoskeleton. *Annu Rev Cell Dev Biol* **21**: 271–295
- Staiger CJ (2000) Signaling to the actin cytoskeleton in plants. *Annu Rev Plant Physiol Plant Mol Biol* **51**: 257–288
- Staiger CJ, Blanchoin L (2006) Actin dynamics: old friends with new stories. *Curr Opin Plant Biol* **9**: 554–562
- Staiger CJ, Gibbon BC, Kovar DR, Zonia LE (1997) Profilin and actin depolymerizing factor: modulators of actin organization in plants. *Trends Plant Sci* **2**: 275–281
- Staiger CJ, Goodbody KC, Hussey PJ, Valenta R, Dröbak BK, Lloyd CW (1993) The profilin multigene family of maize: differential expression of three isoforms. *Plant J* **4**: 631–641
- Staiger CJ, Sheahan MB, Khurana P, Wang X, McCurdy DW, Blanchoin L (2009) Actin filament dynamics are dominated by rapid growth and severing activity in the *Arabidopsis* cortical array. *J Cell Biol* **184**: 269–280
- Suarez C, Carroll RT, Burke TA, Christensen JR, Bestul AJ, Sees JA, James ML, Sirotkin V, Kovar DR (2015) Profilin regulates F-actin network homeostasis by favoring formin over Arp2/3 complex. *Dev Cell* **32**: 43–53
- Sun HQ, Kwiatkowska K, Yin HL (1995) Actin monomer binding proteins. *Curr Opin Cell Biol* **7**: 102–110
- Szymanski DB, Cosgrove DJ (2009) Dynamic coordination of cytoskeletal and cell wall systems during plant cell morphogenesis. *Curr Biol* **19**: R800–R811
- Thomas C (2012) Bundling actin filaments from membranes: some novel players. *Front Plant Sci* **3**: 188
- van Gisbergen PA, Bezanilla M (2013) Plant formins: membrane anchors for actin polymerization. *Trends Cell Biol* **23**: 227–233
- Vidali L, Augustine RC, Kleinman KP, Bezanilla M (2007) Profilin is essential for tip growth in the moss *Physcomitrella patens*. *Plant Cell* **19**: 3705–3722
- Vidali L, Burkart GM, Augustine RC, Kerdavid E, Tüzel E, Bezanilla M (2010) Myosin XI is essential for tip growth in *Physcomitrella patens*. *Plant Cell* **22**: 1868–1882
- Vidali L, van Gisbergen PA, Guérin C, Franco P, Li M, Burkart GM, Augustine RC, Blanchoin L, Bezanilla M (2009) Rapid formin-mediated actin-filament elongation is essential for polarized plant cell growth. *Proc Natl Acad Sci USA* **106**: 13341–13346
- Wang HY, Yu Y, Chen ZL, Xia GX (2005) Functional characterization of *Gossypium hirsutum* profilin 1 gene (*GhPEN1*) in tobacco suspension cells. Characterization of in vivo functions of a cotton profilin gene. *Planta* **222**: 594–603
- Wolven AK, Belmont LD, Mahoney NM, Almo SC, Drubin DG (2000) In vivo importance of actin nucleotide exchange catalyzed by profilin. *J Cell Biol* **150**: 895–904
- Yu JH, Crevenna AH, Bettenbühl M, Freisinger T, Wedlich-Söldner R (2011) Cortical actin dynamics driven by formins and myosin V. *J Cell Sci* **124**: 1533–1541